

Universal precursor seismicity pattern before locked-segment rupture

Hongran Chen^{1,2}, Siqing Qin^{1,2,3*}, Lei Xue^{1,2}, Baicun Yang^{1,2,3} & Ke Zhang^{1,2,3}

Despite the enormous efforts towards searching for precursors, no precursors have exhibited real predictive power with respect to an earthquake thus far. Seismogenic locked segments in a well-defined seismic zone that can accumulate adequate strain energy to cause major earthquakes are very heterogeneous and less brittle. Progressive failures of the locked segments with these properties can produce an interesting seismic phenomenon: a characteristic earthquake and a sequence of smaller subsequent earthquakes (pre-shocks) always arise prior to another characteristic earthquake within the same seismic zone and period. Using a mechanical model, we show that two adjacent characteristic earthquakes reliably occur at the volume-expansion and peak-stress points of a locked segment. Such a seismic pattern has occurred in 62 seismic zones worldwide, suggesting that the pattern applies universally. Both the precursor pattern and the model

¹Key Laboratory of Shale Gas and Geoenvironment, Institute of Geology and Geophysics, Chinese Academy of Sciences, Beijing, China. ²Institutions of Earth Science, Chinese Academy of Sciences, Beijing, China. ³College of Earth and Planetary Sciences, University of Chinese Academy of Sciences, Beijing, China. *e-mail: qsqhope@mail.iggcas.ac.cn

quantifying it permit the prediction of certain characteristic earthquakes in a seismic zone.

In recent decades, there have been many reports of seismological, geodetic, geophysical, geochemical and hydrological precursors to earthquakes¹; however, most of these are physically irrelevant or statistically insignificant. Thus far, no single precursor signal has exhibited real predictive power with respect to a major earthquake^{1,2}. We have analysed the seismic-generation process to identify a reliable signal.

Tectonic earthquakes are widely understood as the brittle failure of local rock accompanied by a rapid release of energy due to fault and plate movement^{3,4}. A major earthquake (e.g. a M_w 8.0 quake) is usually preceded by an intermittent long-term process involving multiscale cracking events in a specified region, whereas the acoustic emissions (AEs) generated from a stressed rock specimen are associated with small-scale cracking events within a short period. Nevertheless, given the similarities in the sequences and statistical distributions of earthquakes and AE events⁴⁻⁷, a primary goal of laboratory studies about AE monitoring is to identify a precursor signal that could be used for earthquake prediction.

Numerous laboratory-scale rock-mechanics experiments⁸⁻¹⁰ have shown that a macroscopic rupture at the peak-stress point (PSP) of a stressed rock specimen is

preceded by the emergence of a volume-expansion point (VEP). The VEP defines the boundary between stable and unstable failure phases⁸. This pattern is essential to the evolution of damage in heterogeneous rocks and provides a physical basis for predicting major earthquakes¹¹. The spatial and temporal (Fig.1) clustering or unstable propagation of micro-cracks beginning at the VEP, as Lockner and Byerlee¹² pointed out, is capable of causing a supra-exponential rise in AE activity that coincides with anomalies in seismic indicators such as wave velocity¹³ and electrical and magnetic signals³. However, these seeming precursors to macroscopic rupture have not been consistently observed in laboratory tests as the mechanical behaviour of a stressed rock specimen and AE activity pattern heavily depend on its heterogeneity, size, shape, and the applied loading conditions. Furthermore, the expansion-related precursor phenomena observed in laboratory settings are not useful for realistic earthquake prediction since recorded spatial and temporal clusters of earthquakes typically do not correspond clearly with a subsequent large event. We argue that when searching for a reliable seismic precursor, one must first understand the physical construct that accumulates high strain energy, and only then can one formulate the related earthquake mechanism.

Many geoscientists^{7,14,15} have recognised that heterogeneous seismogenic faults are composed of both fault gouges and strong local segments that resist slip. Each of the strong segments with high bearing capacity¹⁶ can accumulate enough elastic strain energy to cause major earthquakes. Herein, we refer to such a segment as a 'locked

segment'. Five primary structures fall under this term, illustrated in Fig. 2: a rock bridge, an asperity, a strong junction of two intersecting faults, a locked patch within a creeping segment and a block bounded by secondary faults. These natural locked segments are significantly different from rocks studied in the laboratory in terms of geometric features and tectonic strain rates¹⁷. Seismogenic locked segments are characterised by their large size and flat shape, and they are subjected to shear loading or stress corrosion at an extremely low rate along with high temperatures and high confining pressures. These conditions make seismogenic locked segments highly heterogeneous and less brittle.

Precursor seismicity pattern of locked segment

Several laboratory experiments^{18,19} have demonstrated that even under high confining pressure and temperature, a stressed rock specimen can generate quite a few AEs and fail in a less brittle manner. The premonitory AE activity of a specimen, particularly the event or energy rates at the VEP, can be enhanced if the following conditions are met: the specimen is highly heterogeneous²⁰, it has a small height to diameter ratio²¹ and it is subjected to relatively slow loading²². This trend implies that the precursor seismicity of a large slab-shaped seismogenic locked segment may be unique under similar loading conditions that make the segment less brittle. Indeed, the mechanical behaviour of a seismogenic locked segment, particularly over the long time scales relevant to large-scale tectonic deformation, cannot be modelled realistically in

laboratory tests¹⁷. Nevertheless, field-scale quasi-creep experiments on a locked-segment-like specimen may provide valuable clues in the search for precursor AE activity or seismicity patterns.

An in-situ direct shear test²³ on a large-scale slab-shaped rock block with joints and a loosening seam was performed with slow stress-stepping loading. The geometry and heterogeneity of this block, as well as the loading conditions imposed, were somewhat analogous to those of a natural locked segment. The data in Fig. 3, reprinted from Ishida *et al.*²³, show that the AE event rate rose sharply before the rupture of the block, as expected. This jump in AEs likely corresponds to the emergence of a VEP in a locked segment in the field. After the jump, AEs (pre-shocks) became relatively inactive until the locked segment was damaged to the PSP.

The earth, prone to quakes, is a unique natural laboratory for studying the quake precursor pattern and evolutionary rule. We have observed an interesting phenomenon in a well-defined seismic zone, an area with internally connected seismicity (see Methods), in its current seismic period, exemplified by the Tangshan seismic zone (Fig. 4a or No. 26 in Extended Data Fig. 1 or 2). A characteristic earthquake (CE), i.e. a major earthquake, and a sequence of smaller subsequent earthquakes, which are defined as pre-shocks, always arise prior to another CE (Fig. 4b) (see Extended Data Table 1 or below for names of such earthquakes). Note that the concept of CEs employed herein is wholly different from previous uses of the term, which typically indicates earthquakes with a similar magnitude on a given fault segment that recur at regular

intervals²⁴. A seismicity series comprising two adjacent CEs and pre-shocks between them seemingly resembles the AE activity between the VEP and PSP shown in Fig. 3. In the following analysis, we hypothesise that CEs occur at the VEPs and PSPs of locked segments.

A single seismic period in each seismic zone can be defined by the sequential rupture of all locked segments in ascending order of bearing capacity (low to high). As we hypothesise, when a locked segment is damaged enough that its VEP and PSP are reached, two CEs will appear at the two points, respectively. A seismic zone may have undergone many cycles of seismic periods (Fig. 5) over a long historical course, in each of which the last CE can be referred to as a mainshock. Hence, only those earthquakes occurring exclusively between the mainshock and the onset of the next seismic period are aftershocks.

In the following sections, we describe how we used a theoretical model and case studies drawn from historical data to identify pairs of CEs that occur sequentially at a VEP and a PSP of natural locked segments.

Mechanical model

Several statistical analyses²⁵ have revealed that the ratios of peak strain to volume-expansion strain for rock specimens under uniaxial compression are approximately constant. This constancy probably indicates a mechanical link between the two points.

To study the correlation between the shear strain at the VEP and PSP of a locked segment along a seismogenic fault or a slope slip surface, we have developed a mechanical model that couples a one-dimensional renormalization group model^{15,26,27} with a strain-softening constitutive model^{15,16} based on the Weibull distribution²⁸. This mechanical model^{15,16} is expressed as

$$\frac{\varepsilon_f}{\varepsilon_c} = \left(\frac{2^m - 1}{m \ln 2} \right)^{\frac{1}{m}} \quad (1)$$

where ε_c and ε_f are the shear strain values at the VEP and the PSP of a locked segment and m is the Weibull shape parameter. The shape parameter characterises both the heterogeneity of the rock and its mechanical response to loading conditions, and hence is regarded as a common brittleness index. A smaller m -value indicates that the rock is less brittle. Because the m -values are low for a natural locked segment and lie reasonably within the range of 1.0 to 4.0¹⁶, and the ratio $\varepsilon_f / \varepsilon_c$ is insensitive to variations in the m -value, the ratio can be approximated as a constant 1.48, which is the average value of $\varepsilon_f / \varepsilon_c$ within $m = [1.0, 4.0]$. Thus, equation (1) is approximated as

$$\varepsilon_f = 1.48\varepsilon_c \quad (2)$$

to predict the critical shear strain at the PSP of a locked segment. The model does not require us to determine the specific mechanical parameters of the locked segment in question since we use the constant 1.48.

As a certain seismic zone includes multiple locked segments, the relation¹⁵ derived from equation (2) is as follows:

$$\varepsilon_f(k) = 1.48^k \varepsilon_c \quad (3)$$

where ε_c and $\varepsilon_f(k)$ are the shear strain values corresponding to the VEP of the first locked segment and to the PSP of the k th locked segment, respectively. Note that the shear strain at the PSP of the k th locked segment is approximately equal to the shear strain at the VEP of the $(k + 1)$ th locked segment, indicating that the k th point is both the PSP of the k th locked segment and the VEP of $(k + 1)$ th locked segment. To test the reliability of the model, we have conducted a retrospective analysis of several landslides with locked segments, and we obtained satisfactory results¹⁶.

Based on the assumption that the shear strain within a locked segment is uniformly distributed and unloading shear modulus during a stress drop is approximately equal to the shear elastic modulus of the locked segment²⁹, the cumulative Benioff strain (CBS)³⁰ can be substituted for shear strain in equation (3). Thus, equation (3) becomes as follows:

$$S_f(k) = 1.48^k S_c, \quad (4)$$

where S_c is the CBS value measured at the VEP of the first locked segment, and $S_f(k)$ is the CBS value predicted at the PSP of the k th locked segment.

Because a certain seismic zone ordinarily contains seismic events irrelevant to the progressive failures of locked segments, the minimum validity magnitude M_v ³¹ is set such that an analysis determines the threshold magnitude of the locked segments' cracking and faulting events based on the earthquake catalogue of that zone. M_v is

usually not less than the minimum completeness magnitude M_c^{32} . Particularly before the 1900s, earthquakes whose magnitudes are not smaller than M_v preceding the VEP of the first locked segment were usually not completely recorded. Hence, an initial error in the CBS may be introduced. Therefore, we propose an error-correction expression using equation (4):

$$\Delta = \frac{S_f^*(1) - 1.48S_c^*}{0.48}, \quad (5)$$

where Δ denotes the error, and S_c^* , $S_f^*(1)$ are the uncorrected recorded CBS values at the VEP and PSP of the first locked segment in the zone, respectively.

Case studies

Earthquakes have been recorded across a nearly 3800-year-long period in the intraplate Tangshan seismic zone, which is clearly bounded by several significant deep-seated regional faults³³ (Fig. 4a). Therefore, the Tangshan seismic zone is a strong candidate for ascertaining seismicity characteristics over time and validating our theoretical model. The earthquake catalogues in the Tangshan seismic zone before and after 1900 are drawn from Song *et al.*³⁴ (see Methods) and the China Earthquake Data Center (CEDC). We revised the magnitudes of several large historical events recorded before the invention of instrumentation³⁵ using the rules for magnitude revision described in the Methods. Eleven $M_S \geq 7.0$ earthquakes (Extended Data Table 1) have been recorded in this zone, five of which qualify as CEs under the definition proposed

above (Fig. 4b): 1597-10-06 $M_S7.5$ Bohai Sea earthquake in China (CE1), 1668-07-25 $M_S8.0$ Tancheng earthquake (CE2) in Shandong, 1679-09-02 $M_S7.8$ Sanhe-Pinggu earthquake (CE3) in Hebei, 1888-06-13 $M_S7.8$ Bohai Bay earthquake (CE4) and 1976-07-27 $M_S7.8$ Tangshan earthquake (CE5) in Hebei. The Tangshan earthquake was the largest event recorded in the zone since 1900, and it caused heavy casualties and property damage because of the failure in predicting/forecasting it. If these earthquakes are CEs that indicate VEPs and PSPs of locked segments, their evolutions should match equation (4).

The value of M_v in the Tangshan seismic zone is $M_S5.0$. After the various magnitudes in the record were transformed into a uniform scale (see Methods), the CBS of $M_S \geq 5.0$ earthquakes in this zone was calculated via a widely known formula³⁰. The initial error of CBS was determined using equation (5). Then, the correlation of critical CBS values among CEs in the seismic zone can be quantified using equation (4). The data in Fig. 4c and Table 1 show that the evolutions of these CEs match equation (4) very well, confirming our hypothesis. This shows that the 1597-10-06 $M_S7.5$ Bohai Sea earthquake and the 1668-07-25 $M_S8.0$ Tancheng earthquake form a pair of CEs at the VEP and PSP of the first locked segment. By parity of reasoning, the Tancheng earthquake and the 1679-09-02 $M_S7.8$ Sanhe-Pinggu earthquake form a pair of CEs at the second locked segment in the zone. The first earthquake of each pair of CEs is an identified precursor for the second earthquake in the pair.

In addition, we tested our hypothesis with a retrospective analysis of the inter-plate Hokkaido seismic zone (No. 38 in Extended Data Fig. 1). Shallow-, intermediate- and deep-focus earthquakes have been recorded in this zone. The earthquake catalogues in this zone before and after 1900 were obtained from Song *et al.*³⁴ and the USGS National Earthquake Information Center (NEIC). Three recognisable megathrust CEs are found: the 1898-06-05 $M_{\text{uk}}8.7$ Japan Trench earthquake (CE1), 1952-11-04 $M_{\text{w}}8.9$ earthquake (CE2) off the eastern coast of Kamchatka and 2011-03-11 $M_{\text{w}}9.0$ Tohoku-Oki, Japan earthquake (CE3). Using the same method as we did for the above analysis, we find that pairs of these CEs (Fig. 6 and Table 1) also satisfy equation (4) without modifications of the catalogue. This agreement indicates that brittle failures of locked segments led to the shallow-, intermediate- and deep-focus earthquakes whose magnitudes are not smaller than M_{v} ($M_{\text{v}} = M_{\text{w}}7.0$) recorded in this zone.

Equation (4) has been corroborated by our retrospective analysis of earthquake data (e.g. Extended Data Figs. 3 to 6) in 62 seismic zones (Extended Data Figs. 1 and 2) covering the circum-Pacific seismic belt and the Eurasia seismic belt. The data was drawn from the earthquake catalogue published and revised for consistency (see Methods). The pattern we have identified applies regardless of focal depth, indicating that the precursor pattern is universal. Consequently, we conclude that a CE at the VEP of locked segment reliably precedes the rupture of the segment that leads to a CE at the segment's PSP.

Discussion and prospect

As the damage evolution from the VEP of a locked segment to its PSP usually takes decades or even hundreds of years, the earthquake precursor we have identified can be considered as a long-term precursor. The precursor seismicity pattern and our quantitative mechanical model permit the prediction of CEs within a given seismic zone, except for the first two. Recently, we developed methods for identifying the first foreshock, i.e. a special pre-shock that serves as the indicator of approaching or reaching the critical state of a CE, within a defined seismic zone²⁹, which greatly improves the predictability of CEs and holds great promise for improving earthquake prediction.

Not all major earthquakes can be predicted by our model; CEs with definite physical meanings, except the former two in a seismic period, can be predicted on the basis of firm scientific grounds. Using equation (4) and formulas (6) to (9) (see Methods), one can identify CEs and predict the critical CBS value and magnitude range of a future CE together with the upper-limit magnitude of pre-shocks prior to the said CE within a well-defined seismic zone.

Our work lays the physical foundation for earthquake predictability and has revolutionised the understanding of the earthquake generation process and basic concepts such as mainshock, aftershock, seismic zone and seismic period. When a locked segment is broken, the load applied to it will be mostly transferred to the next locked segment within the same seismic zone, thereby accelerating its failure process.

As the locked segments fail one by one, an increasingly accelerating seismicity trend within this zone is inevitable, as illustrated in Figs. 4c, 6 and Extended Data Figs. 3 to 6. Once the last locked segment with the highest bearing capacity is damaged to its PSP, a mainshock will occur within the same seismic zone and period. This demonstrates that the earthquakes preceding the rupture of the last locked segment are neither mainshocks nor aftershocks, as argued by previous researchers. As each seismic zone evolves towards the critical state of the mainshock, the larger pre-shocks and CEs generated from the stressed locked segments with higher bearing capacity will appear more frequently. Thus, we recommend that countries and regions in seismically active areas should improve the ability to prevent and mitigate earthquake disasters as early as possible.

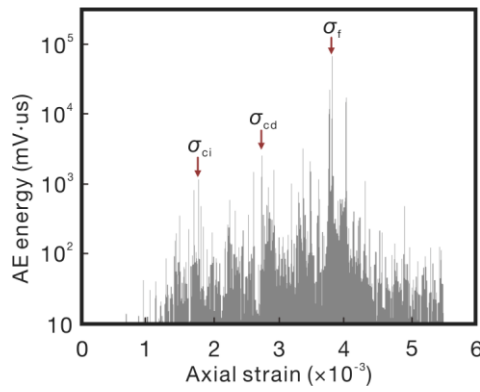


Figure 1 | AE energy vs. strain measured from a granodiorite specimen subjected to uniaxial compression¹⁰. σ_{ci} , σ_{cd} , and σ_f indicate the stress levels corresponding to the crack-initiation point, VEP and PSP, respectively, of the stressed specimen.

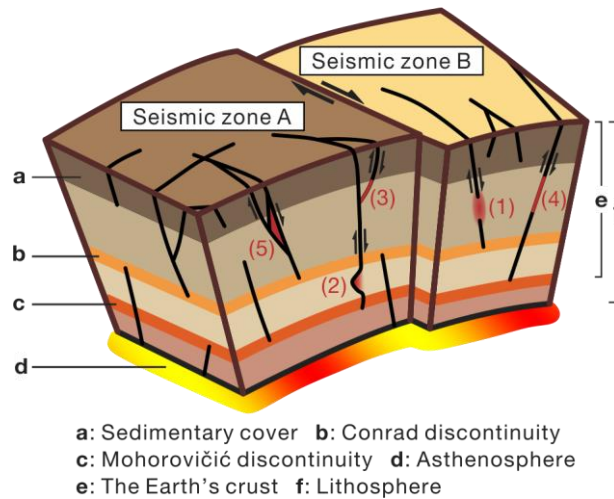


Figure 2 | Illustration of the concepts of intraplate seismic zones and locked

segments. Adjacent tectonic blocks whose corresponding areas are seismic zones, A (light brown) and B (yellowish), are bounded by major faults (thick auburn lines).

Thin black lines represent the secondary faults in a seismic zone. Black arrows denote the movement direction of active faults. Red areas denoted by numerical labels refer to five primary categories of seismogenic locked segments: (1) a rock bridge, (2) an

asperity, (3) a strong junction of two intersecting faults, (4) a locked patch in a creeping segment and (5) a block bounded by secondary faults.

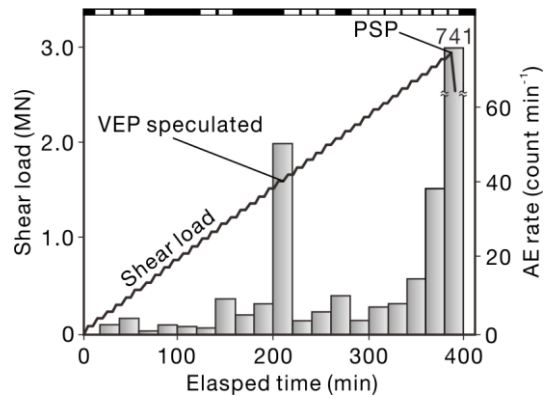
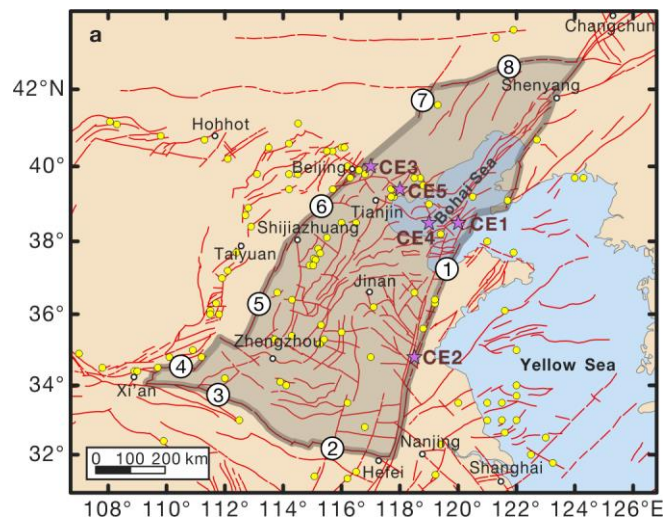


Figure 3 | AE rate (grey bars) and shear load (zigzag line) during an in-situ direct test run²³. The last broken bar denotes an extremely high AE rate, of 741 count·min⁻¹, at the PSP. White and black rectangles at the top of the figure represent the periods with and without AE measurements, respectively.



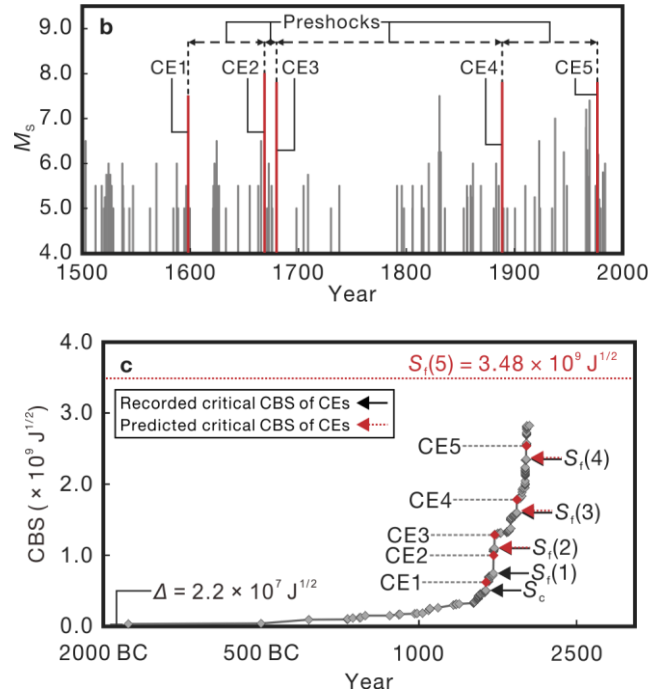


Figure 4 | Seismicity in the Tangshan seismic zone. a, Seismo-tectonic context of

the seismic zone. The seismic zone (shadow area encircled by a closed grey thick curve) is bounded by several major faults (red curves denoted by numerical labels):

- ① Tanlu fault zone; ② Yangce-Gushi-Feizhong fault; ③ Tieluzi-Luanchuan-Nanzhao fault; ④ Huashan Mountain Piedmont fault; ⑤ Taihang Mountain large fault; ⑥ Taihang Mountain piedmont fault; ⑦ Balihan fault; ⑧ Chifeng-Kaiyuan fault.

Yellow solid circles plot the locations of $M_S \geq 6.0$ earthquakes, of which five

CEs (CE1 to CE5) are marked with purple stars. **b**, Time series of $M_S \geq 5.0$

earthquakes. To clarify the CEs, the seismic data between 1500 and 2000 are selected (no $M_S > 7.0$ earthquakes were recorded before 1500 and after 2000). Red bars denote

CE1 to CE5, whose epicentres are marked with red stars in (a). **c**, Time variations of

CBS of $M_S \geq 5.0$ earthquakes from 1767 BC to 19 November 2015, in the seismic

zone and its current seismic period after introducing the initial error Δ . Red diamonds

denote the CEs in **(a)** and **(b)** and grey diamonds denote the other $M_S \geq 5.0$ earthquakes. Table 1 lists the recorded and predicted critical CBS values. The predicted critical CBS value for an expected future CE, calculated from equation (4), is marked with a dotted red line.

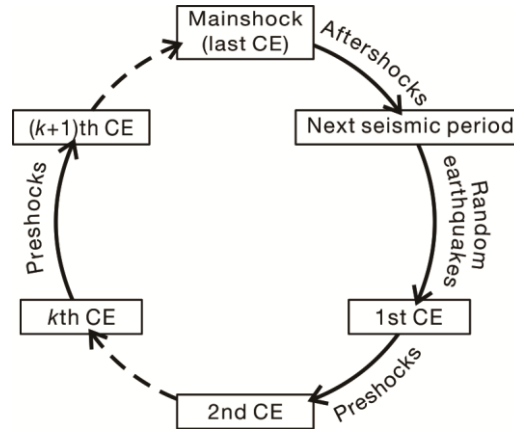


Figure 5 | Cycle of seismic period for a defined seismic zone.

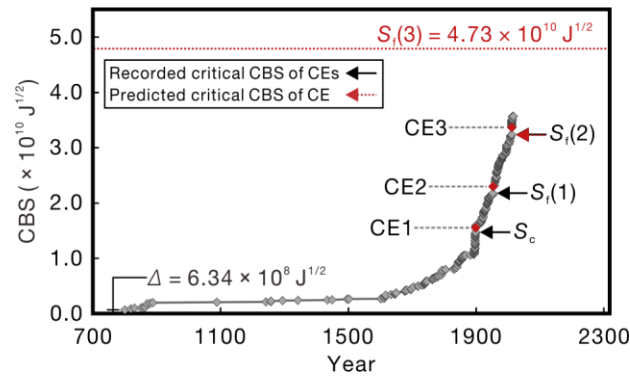


Figure 6 | Time variations of the CBS of $M_w \geq 7.0$ (i.e. $M_v = M_w 7.0$) earthquakes from 15 February 144, to 2 February 2016, in the Hokkaido seismic zone (No. 38 in Extended Data Fig. 1) and its current seismic period after introducing the initial error Δ . Red diamonds mark the CEs, and grey diamonds mark the other $M_w \geq$

7.0 earthquakes. Table 1 lists the recorded and predicted critical CBS values. The predicted critical CBS value for an expected future CE, calculated from equation (4), is marked with a dotted red line.

METHODS

Seismic zoning. The lithosphere of the Earth, as Keilis–Borok³⁶ stated, can be thought of as a hierarchy of blocks with relative movement separated by faults or fault networks at different scales, including tectonic plates^{37–41}, fault blocks^{42,43} and active tectonic blocks^{44,45}. As the strength of a fault is much lower than that of a block, tectonic deformations are concentrated in the boundary faults, while blocks move as a unit with less internal deformation. From this perspective, faults and earthquakes within a tectonic block (e.g. subducting plate) bounded by major faults, or constrained by plate boundaries, are intrinsically linked. Conversely, adjacent blocks only affect the loading or unloading mode of a particular block via shearing or extruding action, but do not affect the intrinsic evolutionary rule reflected in the internal seismicity of the block in question⁴⁶. Thus, a seismic zone can be defined as an area representing the seismicity of a corresponding tectonic block. In previously published works^{35,47,48}, we confirmed that the regular evolution of seismicity with a magnitude equal to or greater than M_v within a seismic zone can represent the unity of a block.

Definitely, our concept of seismic zoning highlights the mechanical interaction between fault networks within a specified seismic zone, which is different from the conventional understanding that earthquakes are related to an individual fault or a fault zone. Relying on data about the faults and plate boundaries illustrated in a seismo-tectonic map^{33,49–52}, we have defined 62 seismic zones

(Extended Data Fig. 1) that cover the circum-Pacific seismic belt and the Eurasia seismic belt, which include 33 seismic zones in China and its neighbouring areas (Extended Data Fig. 2).

Earthquake catalogues. For our case studies regarding 62 seismic zones around the world, we adopted the pre-1900 earthquake catalogue compiled by Song *et al.*³⁴, which is a revised collection of various global catalogues available from authority websites, published books and documents, including $M \geq 5.0$ and $M \geq 6.0$ earthquakes from 9999 BC to 1963 AD and 1964 to May 2011, respectively; the post-1900 earthquake catalogue of earthquakes in China and its neighbouring regions was taken mostly from the CEDC (<http://data.earthquake.cn>), and the post-1900 earthquake catalogue for other regions was compiled from the NEIC database (<http://earthquake.usgs.gov>).

Rules for magnitude revision. Through a comprehensive statistical analysis^{35,47,48} regarding the above earthquake cases, we constrained magnitudes to the following ranges:

$$|M_F - M_C| \leq 0.5 \quad (6)$$

$$M_P \leq \min(M_F, M_C) - 0.2, \quad (7)$$

where M_C and M_F denote the magnitudes of two adjacent CEs before the last CE (mainshock), and M_P denotes the magnitude of pre-shocks between the two adjacent CEs. With regard to double earthquakes, they are viewed as an equivalent earthquake whose seismic energy equals the sum of energy released by them. We have further observed a common pattern in most seismic zones—the magnitudes of several successive CEs before the mainshock usually agree with the following relationship:

$$|M(n+i) - M(n)| \leq 0.2 \quad (n \geq 1) \text{ and } (i \geq 1), \quad (8)$$

where $M(n + i)$ and $M(n)$ indicate the magnitudes of the $(n + i)$ th and n th CEs in a seismic period, respectively.

Once the magnitude scale has been standardised, formulas (6) and (8) can be used to revise and predict the magnitudes of CEs except for a mainshock, and formula (7) can be used to revise and predict the magnitudes of large pre-shocks.

In view of quite a few inaccurate or controversial parameters in earthquake catalogues, particularly magnitude parameters, we standardised the magnitudes^{35,47,48} using formulas (6) to (8) on the basis of several catalogues compiled by individuals and international agencies and research results from some researchers. The revision rules greatly reduce the uncertainty of our earthquake case studies.

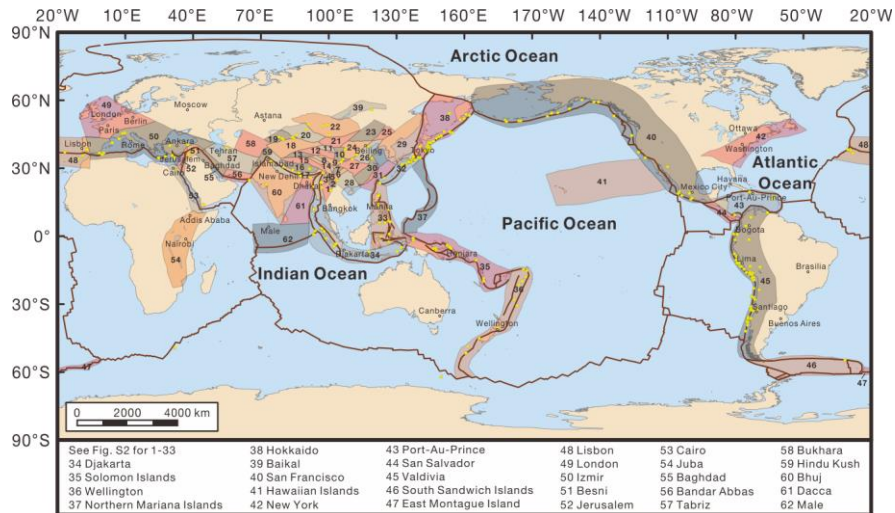
Identification method for a mainshock. Once the last locked segment is damaged to its PSP, a mainshock will occur within the same seismic zone and period. We can identify the mainshock by the following relationship²⁹:

$$M_{F,last} - M_{C,last} > 0.5, \quad (9)$$

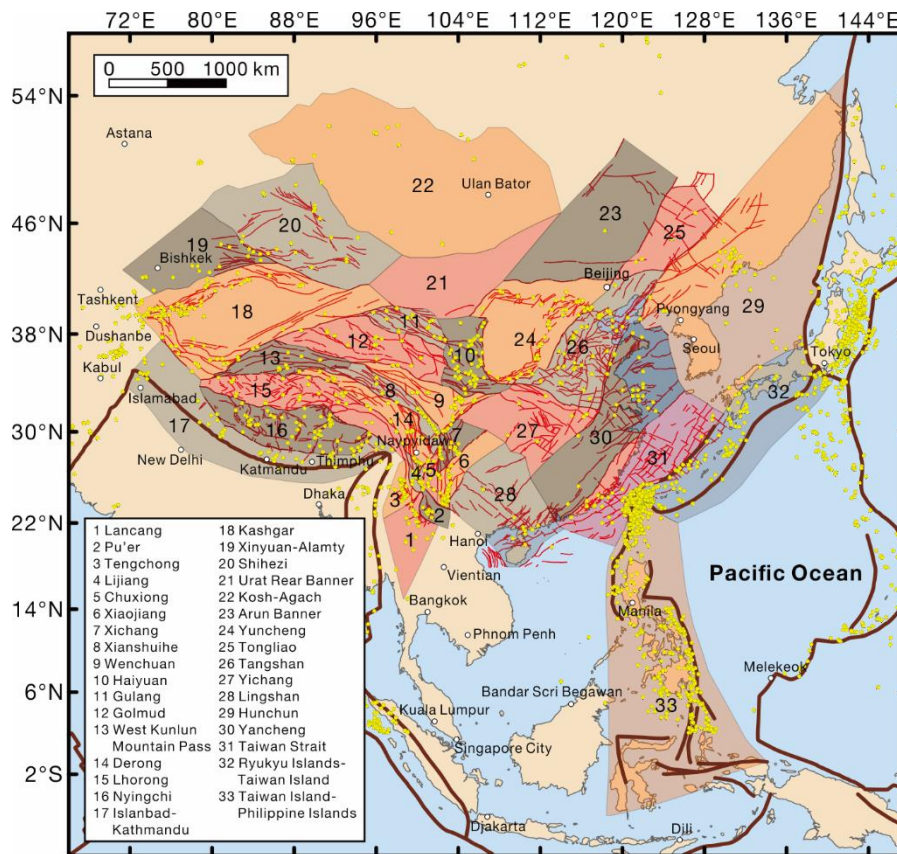
where $M_{C,last}$ and $M_{F,last}$ denote the magnitudes of the CE at the VEP of the last locked segment and the mainshock, respectively.

Conversion between different magnitude scales. Magnitudes are given in the catalogues using several scales, e.g. surface wave magnitude (M_S), short- and long-period body wave magnitudes (m_b and m_B), local magnitude (M_L), moment magnitude (M_W), magnitude defined by the Japan Meteorological Agency (M_j), magnitude calculated statistically (M_{uk}) and magnitudes estimated by the intensity of hazards (M_K) and fault area (M_{fa}). Before calculating CBS, all these magnitudes

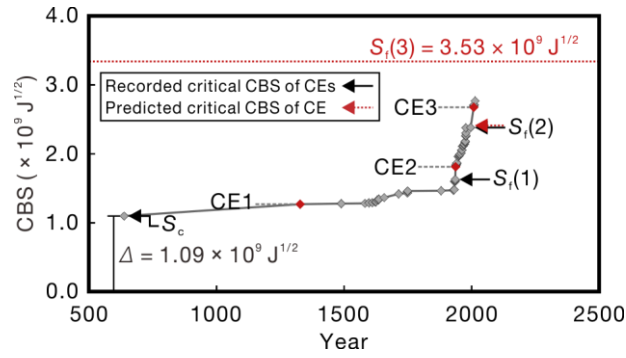
were transformed into a local magnitude scale, M_L , using the appropriate formulas⁵³. Subsequently, we calculated the seismic energy of each event whose magnitude is not less than M_v , the Benioff strain and CBS in turn, using well-known formulas⁵³.



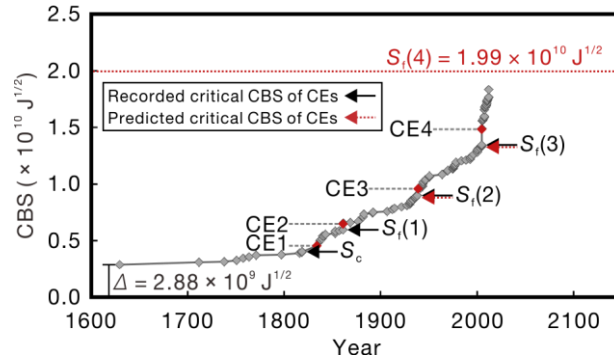
Extended Data Figure 1 | Seismic zoning map including 62 zones (colour shadow areas defined by semi-transparent grey thin curves) worldwide (adapted from Qin *et al.*⁴⁷). Numerical labels in black bold font are attached to each zone; the zone names corresponding to these numbers are listed in the bottom table. Data concerning the tectonic plate boundaries (auburn curves) were taken from the NEIC database (<http://earthquake.usgs.gov>, last accessed on 11 September 2014). Yellow solid circles plot the locations of $M \geq 8.0$ earthquakes.



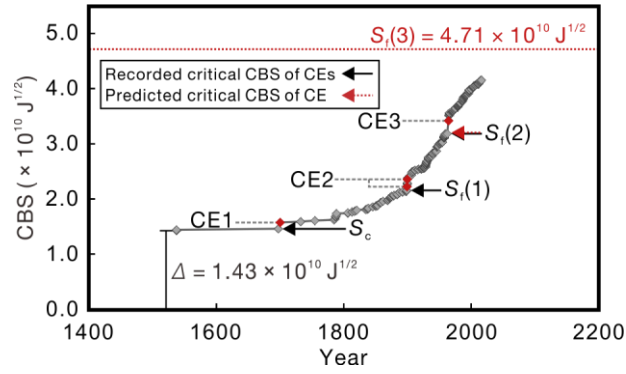
Extended Data Figure 2 | Seismic zoning map including 33 zones (colour shadow areas defined by semi-transparent grey thin curves) in China and its neighbouring areas (adapted from Qin *et al.*³⁵). Each zone is labelled with a number in black font; the zone names corresponding to these numbers are listed in the bottom-left table. The fault data (red curves) are from the Map of Active Tectonic in China³³ and the data of tectonic plate boundaries (thick auburn curve) are from the NEIC (<http://earthquake.usgs.gov>, last accessed on 11 September 2014). Yellow solid circles plot the locations of $M \geq 6.0$ earthquakes.



Extended Data Figure 3 | Time variations of CBS of $M_S \geq 5.5$ (i.e. $M_v = M_S5.5$) earthquakes from 14 February 638, to 21 August 2017, in the Wenchuan seismic zone (No. 9 in Extended Data Figure 1 or 2) and its current seismic period after introducing the initial error Δ . Red diamonds denote the CEs and grey diamonds denote the other $M_S \geq 5.5$ earthquakes. The CEs in this zone are the 1327-09 $M_S7.75$ Tianquan earthquake (CE1) in Sichuan, 1937-01-07 $M_S7.8$ Maduo earthquake (CE2) in Qinhai and 2008-05-12 $M_S8.1$ Wenchuan earthquake (CE3) in Sichuan. The predicted critical CBS value for an expected future CE, calculated from equation (4), is marked with a dotted red line.

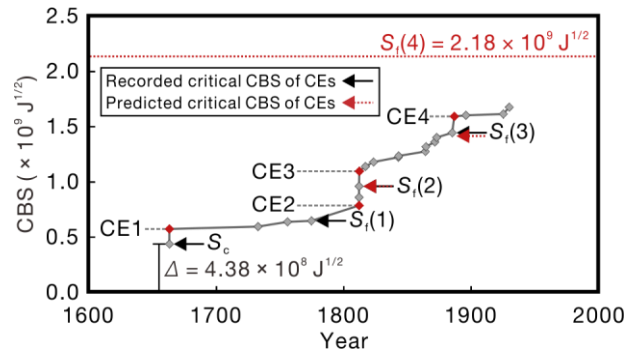


Extended Data Figure 4 | Time variations of CBS of $M_w \geq 7.0$ (i.e. $M_v = M_w 7.0$) earthquakes from 1 August 1629, to 27 February 2015, in the Djakarta seismic zone (No. 34 in Extended Data Figure 1) and its current seismic period after introducing the initial error Δ . Red diamonds denote CEs, and grey diamonds denote the other $M_w \geq 7.0$ earthquakes. The CEs in this zone are the 1818-11-08 $M_s 8.5$ earthquake (CE1) in Bali Sea, 1861-02-16 $M_s 8.5$ Simuk, Indonesia earthquake (CE2), 1938-02-01 $M_w 8.5$ Banda Sea earthquake (CE3) and 2004-12-26 $M_w 9.0$ Simeulue Island earthquake (CE4). The predicted critical CBS value for an expected future CE, calculated from equation (4), is marked with a dotted red line.



Extended Data Figure 5 | Time variations of CBS of $M_W \geq 7.0$ (i.e. $M_v = M_W 7.0$) earthquakes from 20 December 1523, to 24 February 2016, in the San Francisco seismic zone (No.40 in Extended Data Figure 1) and its current seismic period after introducing the initial error Δ .

Red diamonds denote the CEs and grey diamonds denote the other $M_W \geq 7.0$ earthquakes. The CEs in this zone are the 1700-01-26 $M_S 9.0$ earthquake (CE1) near coast of west Oregon, USA, 1899-01-04 $M_{uk} 8.6$ and 1899-09-10 $M_W 8.6$ double earthquakes occurring in Guerrero-Oaxaca, Mexico and Gulf of Alaska, USA, respectively, whose releasing energy is equivalent to that of a $M_W 8.8$ event (CE2), and 1964-03-28 $M_W 9.3$ Alaska earthquake (CE3). The predicted critical CBS value for an expected future CE, calculated from equation (4), is marked with a dotted red line.



Extended Data Figure 6 | Time variations of CBS of $M_w \geq 6.0$ (i.e. $M_v = M_w 6.0$) earthquakes from 27 December 1568, to 15 February 2014, in the New York seismic zone (No.42 in

Extended Data Figure 1) and its current seismic period after introducing the initial error Δ .

Red diamonds denote the CEs and grey diamonds denote the other $M_w \geq 6.0$ earthquakes. The CEs in this zone are the 1663-02-05 $M_S 7.6$ St Lawrence Valley, Canada earthquake (CE1), 1811-12-16 $M_S 7.6$ earthquake (CE2) and 1812-02-07 $M_S 7.6$ earthquake (CE3) in New Madrid, USA and 1886-09-01 $M_w 7.7$ Charleston, USA earthquake (CE4). The predicted critical CBS value for an expected future CE, calculated from equation (4), is marked with a dotted red line.

Extended Data Table 1 | $M_s \geq 7.0$ earthquakes in the Tangshan seismic zone of which five**CEs are indicated with red text.**

No.	Date	Latitude and Longitude (°)	Magnitude (M_s)	Location
1	70 BC-06-01	36.30 N, 119.20 E	7.0	Zhucheng, Shandong
2	1597-10-06	38.50N, 120.00E	7.5	Bohai Sea
3	1668-07-25	34.80N, 118.50E	8.0	Tancheng, Shandong
4	1668-07-26	36.40N, 119.20E	7.0	Anqiu, Shandong
5	1679-09-02	40.00N, 117.00E	7.8	Sanhe-Pinggu, Hebei
6	1830-06-12	36.40N, 114.30E	7.5	Cixian, Hebei
7	1888-06-13	38.50N, 119.00E	7.8	Bohai Bay
8	1937-08-01	35.20N, 115.30E	7.0	Heze, Shandong
9	1966-03-22	37.50N, 115.10E	7.2	Xingtai, Hebei
10	1969-07-18	38.20N, 119.40E	7.4	Bohai Sea
11	1976-07-27	39.40N, 118.00E	7.8	Tangshan, Hebei
12	1976-07-28	39.70N, 118.50E	7.5	Luanxian, Hebei

References

1. Hough, S. *Predicting the Unpredictable: the Tumultuous Science of Earthquake Prediction* (Princeton: Princeton University Press, 2010)
2. Kagan, Y. Y. Are earthquakes predictable? *Geophys J Int* **131**, 505–525.
<http://dx.doi.org/10.1111/j.1365-246X.1997.tb06595.x> (1997).

3. Byerlee, J. A review of rock mechanics studies in the United States pertinent to earthquake prediction. *PAGEOPH* **116**, 586–602.
<http://dx.doi.org/10.1007/BF00876526> (1978).
4. Vallianatos, F., Michas, G., Benson, P. & Sammonds, P. Natural time analysis of critical phenomena: the case of acoustic emissions in triaxially deformed Etna basalt. *Phys A* **392**, 5172–5178.
<http://dx.doi.org/10.1016/j.physa.2013.06.051> (2013).
5. Davidsen, J., Stanchits, S. & Dresen, G. Scaling and universality in rock fracture. *Phys Rev Lett* **98**, 125502.
<http://dx.doi.org/10.1103/PhysRevLett.98.125502> (2007).
6. Hirata, T. Omori's Power Law aftershock sequences of microfracturing in rock fracture experiment. *J Geophys Res* **92**, 6215–6221.
<http://dx.doi.org/10.1029/JB092iB07p06215> (1987).
7. Lei, X. How do asperities fracture? An experimental study of unbroken asperities. *Earth Planet Sci Lett* **213**, 347–359.
[http://dx.doi.org/10.1016/S0012-821X\(03\)00328-5](http://dx.doi.org/10.1016/S0012-821X(03)00328-5) (2003).
8. Alkan, H., Cinar, Y. & Pusch, G. Rock salt dilatancy boundary from combined acoustic emission and triaxial compression tests. *Int J Rock Mech Min Sci* **44**, 108–119. <http://dx.doi.org/10.1016/j.ijrmms.2006.05.003> (2007).

9. Brace, W. F., Paulding, B. W. & Scholz, C. Dilatancy in the fracture of crystalline rocks. *J Geophys Res* **71**, 3939–3953.
<http://dx.doi.org/10.1029/JZ071i016p03939> (1966).
10. Zhao, X. et al. in the 3rd ISRM SINOROCK Symposium (eds Feng, Xiating, Hudson, J. A. & Tan, F.) 75–80 (CRC Press)
11. Scholz, C. H., Sykes, L. R. & Aggarwal, Y. P. Earthquake prediction: a physical basis. *Science* **181**, 803–810.
<http://dx.doi.org/10.1126/science.181.4102.803>. [17816227](https://doi.org/10.1126/science.181.4102.803) (1973).
12. Lockner, D. A. & Byerlee, J. D. Acoustic emission and creep in rock at high confining pressure and differential stress. *Bull Seismol Soc Am* **67**, 247–258 (1977)
13. Scholz, C. H. Velocity anomalies in dilatant rock. *Science* **201**, 441–442.
<http://dx.doi.org/10.1126/science.201.4354.441>. [17729897](https://doi.org/10.1126/science.201.4354.441) (1978).
14. Aki, K. Asperities, barriers, characteristic earthquakes and strong motion prediction. *J Geophys Res* **89**, 5867–5872.
<http://dx.doi.org/10.1029/JB089iB07p05867> (1984).
15. Qin, S. et al. Brittle failure mechanism of multiple locked patches in a seismogenic fault system and exploration on a new way for earthquake prediction. *Chin J Geophys* **53**, 1001–1014 (2010)

16. Chen, H., Qin, S., Xue, L., Yang, B. & Zhang, K. A physical model predicting instability of rock slopes with locked segments along a potential slip surface. *Eng Geol* **242**, 34–43. <http://dx.doi.org/10.1016/j.enggeo.2018.05.012> (2018).
17. Brantut, N., Heap, M. J., Meredith, P. G. & Baud, P. Time-dependent cracking and brittle creep in crustal rocks: a review. *J Struct Geol* **52**, 17–43. <http://dx.doi.org/10.1016/j.jsg.2013.03.007> (2013).
18. Chernak, L. J. & Hirth, G. Deformation of antigorite serpentinite at high temperature and pressure. *Earth Planet Sci Lett* **296**, 23–33. <http://dx.doi.org/10.1016/j.epsl.2010.04.035> (2010).
19. Shimada, M. Confirmation of two types of fracture in granite deformed at temperatures to 300°C. *Tectonophysics* **211**, 259–268. [http://dx.doi.org/10.1016/0040-1951\(92\)90063-C](http://dx.doi.org/10.1016/0040-1951(92)90063-C) (1992).
20. Mogi, K. Study of elastic shocks caused by the fracture of heterogeneous materials and its relation to earthquake phenomena. *Bull Earthquake Res Inst Univ Tokyo* **40**, 125–173 (1962)
21. Meng, Q., Zhang, M., Han, L., Pu, H. & Li, H. Effects of size and strain rate on the mechanical behaviors of rock specimens under uniaxial compression. *Arab J Geosci* **9**, 527. <http://dx.doi.org/10.1007/s12517-016-2559-7> (2016).
22. Baud, P. & Meredith, P. G. Damage accumulation during triaxial creep of Darley Dale sandstone from pore volumetry and acoustic emission. *Int J*

- Rock Mech Min Sci* **34**, 24.e1–24.e10. [http://dx.doi.org/10.1016/S1365-1609\(97\)00060-9](http://dx.doi.org/10.1016/S1365-1609(97)00060-9) (1997).
23. Ishida, T., Kanagawa, T. & Kanaori, Y. Source distribution of acoustic emissions during an in-situ direct shear test: implications for an analog model of seismogenic faulting in an inhomogeneous rock mass. *Eng Geol* **110**, 66–76. <http://dx.doi.org/10.1016/j.enggeo.2009.11.003> (2010).
24. Schwartz, D. P. & Coppersmith, K. J. Fault behavior and characteristic earthquakes: examples from the Wasatch and San Andreas Fault Zones. *J Geophys Res* **89**, 5681–5698. <http://dx.doi.org/10.1029/JB089iB07p05681> (1984).
25. Xue, L. et al. A potential strain indicator for brittle failure prediction of low-porosity rock: Part II—Theoretical Studies Based on Renormalization Group Theory. *Rock Mech Rock Eng* **48**, 1773–1785. <http://dx.doi.org/10.1007/s00603-014-0681-y> (2015).
26. Smalley, R. F., Turcotte, D. L. & Solla, S. A. A renormalization group approach to the stick-slip behavior of faults. *J Geophys Res* **90**, 1894–1900. <http://dx.doi.org/10.1029/JB090iB02p01894> (1985).
27. Xue, L. et al. A potential strain indicator for brittle failure prediction of low-porosity rock: Part I—Experimental Studies Based on the Uniaxial Compression Test. *Rock Mech Rock Eng* **48**, 1763–1772. <http://dx.doi.org/10.1007/s00603-014-0675-9> (2015).

28. Weibull, W. A statistical distribution function of wide applicability. *J Appl Mech* **13**, 293–297 (1951)
29. Yang, B. A Physical Self-Similarity Law Describing the Accelerating Failure Behavior of Locked Segments PhD thesis (University of Chinese Academy of Sciences, 2019)
30. Benioff, H. Earthquakes and rock creep (Part I: creep characteristics of rocks and the origin of aftershocks). *Bull Seismol Soc Am* **41**, 31–62 (1951)
31. Qin, S., Yang, B., Xue, L., Li, P. & Wu, X. Prospective prediction of major earthquakes for the Taiwan Strait seismic zone. *Prog Geophys* **30**, 2013–2019 (2015)
32. Wiemer, S. & Wyss, M. Minimum magnitude of completeness in earthquake catalogs: examples from Alaska, the Western United States, and Japan. *Bull Seismol Soc Am* **90**, 859–869. <http://dx.doi.org/10.1785/0119990114> (2000).
33. Deng, Q., Ran, Y., Yang, X., Min, W. & Chu, Q. *Map of Active Tectonic in China (1:4000000)* (Beijing: Seismological Press, 2007)
34. Song, Z., Zhang, G. & Liu, J. *Global Earthquake Catalog* (Beijing: Seismological Press, 2011)
35. Qin, S., Yang, B., Wu, X., Xue, L. & Li, P. The identification of mainshock events for some seismic zones in mainland China (II). *Prog Geophys* **31**, 115–142 (2016)

36. Keilis-Borok, V. I. Symptoms of instability in a system of earthquake-prone faults. *Phys D* **77**, 193–199. [http://dx.doi.org/10.1016/0167-2789\(94\)90133-3](http://dx.doi.org/10.1016/0167-2789(94)90133-3) (1994).
37. Le Pichon, X. Sea-floor spreading and continental drift. *J Geophys Res* **73**, 3661–3697. <http://dx.doi.org/10.1029/JB073i012p03661> (1968).
38. McKenzie, D. P. & Parker, R. L. The North Pacific: an example of tectonics on a sphere. *Nature* **216**, 1276–1280. <http://dx.doi.org/10.1038/2161276a0> (1967).
39. Morgan, W. J. Rises, trenches, great faults, and crustal blocks. *J Geophys Res* **73**, 1959–1982. <http://dx.doi.org/10.1029/JB073i006p01959> (1968).
40. Wilson, J. T. A new class of faults and their bearing on continental drift. *Nature* **207**, 343–347 (1965). [10.1038/207343a0](https://doi.org/10.1038/207343a0)
41. Wilson, J. T. Did the Atlantic close and then re-open? *Nature* **211**, 676–681. <http://dx.doi.org/10.1038/211676a0> (1966).
42. Zhang, W., Li, Y., Zhong, J. & Ma, F. Fracture systems and fault-block tectonics. *Sci Sin* **24**, 1717 (1981)
43. Zhang, W., Ye, H. & Zhong, J. On “fault blocks” and “plates”. *Sci Sin* **22**, 1406 (1979)
44. Zhang, G., Ma, H., Wang, H. & Wang, X. Boundaries between active-tectonic blocks and strong earthquakes in China mainland. *Chinese J Geophys* **48**, 662–671. <http://dx.doi.org/10.1002/cjg2.699> (2005).

45. Zhang, P. et al. Active tectonic blocks and strong earthquakes in the continent of China. *Sci China Ser D* **46**, 13–24 (2003)
46. Wu, X. et al. Physical mechanism of major earthquakes by earthquake cases. *Chin J Geophys* **59**, 3696–3710 (2016)
47. Qin, S., Li, P., Yang, B., Xue, L. & Wu, X. The identification of mainshock events for main seismic zones in seismic belts of the Circum Pacific, ocean ridge and continental rift. *Prog Geophys* **31**, 574–588 (2016)
48. Qin, S., Yang, B., Xue, L., Li, P. & Wu, X. The identification of mainshock events for main seismic zones in the Eurasian seismic belt. *Prog Geophys* **31**, 559–573 (2016)
49. Li, T., Geng, S., Yan, K., Fan, B. & Chen, B. *Geological Map of Asia and Europe (1:5000000)* (Beijing: Geological Publishing House, 1997)
50. Miao, P. & Zhou, X. *Global Tectonic Systems Map (1:25000000)* (Beijing: Seismological Press, 2010)
51. Shen, J., Bai, M., Shi, G. & Рогожкин, Е. А. *Map of Seismotectonics in the Xinjiang and Its Adjacent Areas (1:2500000)* (Wuhan, Hubei: China: University of Geoscience, 2014)
52. Zhang, Y., Wang, L. & Dong, R. *Seismotectonic Map of Asia and Europe (1:8000000)* (Beijing: Cartographic Publishing House, 1981)

53. Yang, B., Qin, S., Xue, L., Wu, X. & Zhang, K. On the equivalence between the cumulative Benioff strain and the shear strain for the locked patches along a seismogenic fault system. *Prog Geophys* 32, 1067–1070 (2017)

Acknowledgements We thank S. Wang and J. Yang of the Institute of Geology and Geophysics, Chinese Academy of Sciences, for their valuable comments and suggestions. This work was supported by the National Natural Science Foundation of China to S. Q. (grant 41572311 and U1704243) and L. X. (grant 41302233), and by the China Postdoctoral Science Foundation (grant 2018M640181) to H. C.

Author contributions S. Q. initiated the study. S. Q. and H. C. conceived the idea of this study. L. X., B. Y. and K. Z. analysed the data. H. C. and L. X. interpreted the results. H. C. wrote the original manuscript. All authors discussed the results and revised the manuscript.

Competing interests The authors declare that they have no competing interests.

Correspondence and requests for materials should be addressed to S. Q.

Data and codes availability Sources of all the data needed to evaluate the conclusions in the paper are present in the paper and/or the Methods. Additional data related to the findings of this study are available from the corresponding author upon reasonable request.

Tables

Table 1 | Recorded and predicted critical CBS values corresponding to the predictable CEs in Tangshan (Fig. 4c) and Hokkaido (Fig. 6) seismic zones.

Names of seismic zones	CE	Recorded CBS value ($J^{1/2}$)	Predicted CBS value ($J^{1/2}$)
Tangshan	CE3	1.10×10^9	1.11×10^9
	CE4	1.60×10^9	1.63×10^9
	CE5	2.35×10^9	2.37×10^9
Hokkaido	CE3	3.24×10^{10}	3.23×10^{10}